FEBS Letters 588 (2014) 1873–1878

FEBS Letters

journal homepage: www.FEBSLetters.org

The cytochrome *c* peroxidase and cytochrome *c* encounter complex: The other side of the story

Jesika Schilder [a], Frank Löhr [b], Harald Schwalbe [c], Marcellus Ubbink [a,*]

[a] *Leiden Institute of Chemistry, Gorlaeus Laboratories, Leiden University, Einsteinweg 55, 2333 CC Leiden, The Netherlands*
[b] *Institute of Biophysical Chemistry, Goethe University Frankfurt and Centre for Biomolecular Magnetic Resonance, Max-von-Laue Strasse 9, 60438 Frankfurt am Main, Germany*
[c] *Institute of Organic Chemistry and Chemical Biology, Goethe University Frankfurt and Centre for Biomolecular Magnetic Resonance, Max-von-Laue Strasse 7, 60438 Frankfurt am Main, Germany*

ARTICLE INFO

Article history:
Received 10 February 2014
Revised 18 March 2014
Accepted 26 March 2014
Available online 12 April 2014

Edited by Miguel De la Rosa

Keywords:
Paramagnetic NMR
Spin label
Transient complex
Paramagnetic relaxation enhancement
Protein complex
Electron transfer

ABSTRACT

Formation of an encounter complex is important for efficient protein complex formation. The encounter state consists of an ensemble of orientations of two proteins in the complex. Experimental description of such ensembles inherently suffers from insufficient data availability. We have measured paramagnetic relaxation enhancements (PRE) on cytochrome *c* peroxidase (CcP) caused by its partner cytochrome *c* (Cc) carrying a spin label. The data complement earlier PRE data of spin labelled CcP, identifying several new interactions. This work demonstrates the need of obtaining as many independent data sets as possible to achieve the most accurate description of an encounter complex.

Structured summary of protein interactions:
CcP and **Cc** bind by nuclear magnetic resonance (View interaction)

© 2014 Federation of European Biochemical Societies. Published by Elsevier B.V. All rights reserved.

1. Introduction

1.1. The encounter complex and the inverse problem

Protein–protein complex formation requires an intermediary complex to form before the final, stereospecific state is reached. The formation of this encounter complex is driven by long-range charge–charge and hydrophobic interactions, resulting in a weakly associated complex in which the protein partners are free to rotate and reorient themselves. From there, the number of short-range interactions (van der Waals, hydrogen-bonding, hydrophobic interactions and salt bridges) between the pair is increased to form the stereospecific state [1].

The transient and highly dynamic nature of the encounter complex makes it difficult to observe and visualize. Because the encounter complex is comprised of a large number of transient, low energy and weakly interacting conformations, it is essentially invisible to many structural biology techniques. Paramagnetic nuclear magnetic resonance (NMR) spectroscopy provides a unique opportunity to study these highly dynamic complexes as the observed effects, from paramagnetic relaxation enhancement (PRE) in particular, are extremely sensitive for those lowly populated states in which the nucleus is closer to a paramagnetic centre than in the other state(s) [2].

The main drawback is that the PRE, like many other NMR observables, is an average over all the conformations present in the sample. This makes visualization of the complex an *ill-posed inverse problem* [3,4], in which many ensembles of solutions can be found to match the observed data [5–14]. In fact, the only result that can be determined conclusively is where the interaction does not occur. If a paramagnetic centre does not cause PRE on the partner, it can be concluded that the surface region around that centre is not sampled by the partner for a significant fraction of the lifetime of the complex. Therefore, by using paramagnetic probes at several locations on the protein's surface, an exclusion map can be generated [5–7,14–16]. The more restraints can be incorporated into the modelling calculations, the more refined the ensemble of structures becomes and the closer it will be to the true ensemble in the sample [17–21].

Abbreviations: Cc, cytochrome *c*; CcP, cytochrome *c* peroxidase; CSP, chemical shift perturbations; I_{para}/I_{dia}, intensity ratio; MTS, 1-acetoxy-2,2,5,5-tetramethyl-δ3-pyrroline-3-methyl)-methanethiosulfonate; MTSL, 1-oxyl-2,2,5,5-tetramethyl-δ3-pyrroline-3-methyl)-methanethiosulfonate; NaPi, sodium phosphate; PRE, paramagnetic relaxation enhancement; $\Delta\delta_{avg}$, average CSP

* Corresponding author. Fax: +31 71 5275856.
E-mail address: m.ubbink@chem.leidenuniv.nl (M. Ubbink).

http://dx.doi.org/10.1016/j.febslet.2014.03.055
0014-5793/© 2014 Federation of European Biochemical Societies. Published by Elsevier B.V. All rights reserved.

1.2. The cytochrome c peroxidase–cytochrome c complex

Encounter complexes are highly populated in complexes that represent a compromise between specific binding and high-turnover. Therefore, electron transport complexes are ideal candidates for studying the encounter complex as they require binding specific enough to allow for electron transfer but weak and transient enough to accommodate very high turn-over rates [22]. The electron transfer complex between yeast *iso*-1-cytochrome *c* (Cc) and yeast cytochrome *c* peroxidase (CcP) is a well characterized system for studying the encounter complex. It spends approximately 30% of the time in the encounter complex [5,15], which can be shifted to as low as 10% or as high as 90% with point mutations near the binding interface [23].

The solution structure of the CcP–Cc encounter complex was determined in 2006 by Volkov et al. using PRE effects generated in the ^{15}N-HSQC spectra of Cc by MTSL spin labels attached at five locations on the surface of CcP [15]. Although both of these proteins contain a paramagnetic haem group, the effects produced by these are not suitable for studying the complex. Therefore, MTSL spin labels were used to generate PREs, which provided restraints for docking of the proteins. The study demonstrated that the complex spends approximately 70% of the time in the stereospecific state found in the crystal structure [24] and 30% in other orientations representing the encounter complex. The model of the latter was later refined by Bashir et al. in 2010 by expanding the initial data to include PRE restraints from MTSL attached at ten sites on CcP. Back-calculated data from a theoretical encounter complex, generated using an electrostatics based Monte Carlo method, was compared to the experimental PREs. The additional data obtained allowed for the complete mapping of the conformational space sampled; Cc was found to sample only 15% of the CcP surface during complex formation [5], in line with the results from earlier theoretical studies [25,26].

The goal of the present study was to view the CcP–Cc encounter complex from "the other side" and validate the previously determined ensemble. The NMR resonances of the backbone amides of CcP (34.2 kDa) were assigned, which then allowed us to observe both chemical shift perturbations (CSP) and PRE effects in the NMR spectrum of CcP that were generated in the presence of spin-labelled Cc. We observe many effects similar to those previously reported for the complex as well as several novel interactions. These results show the importance of extending the available set of restraints as far as possible to increase the accuracy of an encounter complex description.

2. Material and methods

2.1. Sub-cloning of yeast CcP

The gene construct for *Saccharomyces cerevisiae* CcP C128A [15] was sub-cloned into a pET28a(+) vector. The gene was amplified using PCR with a 5′ primer containing a *Pci*I site (resulting in MSKT as the first four amino acids) and a 3′ primer containing an *Xho*I site. The fragment was cloned into a pET28a(+) vector cut with *Xho*I and *Nco*I, which are compatible with *Pci*I, yielding pET28aCcP. The sequence of the insertion was verified by DNA sequencing.

2.2. Expression and purification of CcP

The pET28aCcP plasmid was used to express and purify CcP in a protocol adapted from Refs. [27,28] with changes for labelled protein expression and the use of phosphate buffers, see Supplementary Methods for details. The concentration of CcP was determined using UV–Vis spectroscopy at $\varepsilon_{408nm} = 98\ mM^{-1}cm^{-1}$ and the coordination of the haem group was determined using several absorbance ratios [29].

2.3. Protein expression and purification of Cc

A pUC19 based plasmid containing the *S. cerevisiae* iso-1-cytochrome *c* gene was used to express and purify Cc as described previously [30,31]. The wild type (WT) protein and mutant V28C [9] were used. The concentration of Cc was determined using UV–Vis spectroscopy and $\varepsilon_{410nm} = 106.1\ mM^{-1}cm^{-1}$ [31]. The standard yield was approximately 20 mg/L in rich media for both WT and V28C Cc.

2.4. Spin-labelling

Samples of V28C Cc were labelled with either MTS [1-acetoxy-2,2,5,5-tetramethyl-δ3-pyrroline-3-methyl)-methanethiosulfonate] or MTSL [1-oxyl-2,2,5,5-tetramethyl-δ3-pyrroline-3-methyl)-methanethiosulfonate] (Toronto Research Chemicals, North York, ON, Canada) as described previously [15], see Supplementary Methods for details. The labelling efficiency was determined by mass spectroscopy to be essentially 100%.

2.5. NMR spectroscopy

2.5.1. CcP assignment

CcP appears to be stable at 20 °C for only 4–5 days, so several samples were required for the backbone assignment experiments. A large sample of 400 μM triple labelled [^{15}N, ^{13}C, ^{2}H] CcP was prepared in 20 mM sodium phosphate (NaPi), 100 mM NaCl, 6% D_2O, pH 6.0 and then aliquoted into several identical samples. A full set of protein amide backbone assignment experiments were recorded and processed at the Biomolecular Magnetic Resonance facility, Goethe University, Frankfurt. The data was processed using Topspin 3.1 (Bruker, Karlsruhe, Germany) and spectral assignment and analysis was done using CCPN analysis 2.1.5 [32]. See Supplementary Methods for details. NMR assignments have been submitted to the BMRB under entry number 19884.

2.5.2. Titration experiments

To obtain binding constants, 1.7–2.5 mM stocks of WT or MTS-V28C Cc were titrated into 400 μM double labelled [^{15}N, ^{2}H] CcP in 20 mM NaPi, 100 mM NaCl, 6% D_2O, pH 6.0. 2D BEST-TROSY-HSQC experiments [33] were recorded on a Bruker AVIII HD spectrometer equipped with a ^{1}H{^{13}C/^{15}N} TCI-cryoprobe operating at a Larmor frequency of 850 MHz at 293 K with 1024 and 100 complex points in the ^{1}H and ^{15}N dimensions, respectively. Spectra were recorded at intervals of 0.2:1 Cc:CcP until a final ratio of Cc:CcP of 2.0:1 was reached. All data were processed using Topspin 3.2 (Bruker, Karlsruhe, Germany) and analysis was done using CCPN Analysis 2.1.5.

The average CSP ($\Delta\delta_{avg}$) were derived as described previously [34]. With the derived binding constants, it was calculated that 98% of WT or 99% V28C Cc was bound to CcP, in the sample with a 2:1 ratio of Cc:CcP. Therefore, in order to obtain $\Delta\delta_{avg}$ extrapolated to the 100% bound form, the respective $\Delta\delta_{avg}$ values were divided by 0.98 or 0.99. The chemical shift titration curves were analyzed with a two-parameter, non-linear least squares fit using a one-site binding model as described previously [35]. The fitting was done using OriginPro 8.5 (OriginLab, Northampton, USA).

2.5.3. Paramagnetic experiments

NMR samples contained 400 μM double labelled [^{15}N, ^{2}H] CcP in 20 mM NaPi, 100 mM NaCl, 6% D_2O, pH 6.0 with either 120 μM or 290 μM MTS(L)-V28C Cc. 2D BEST-TROSY-HSQC experiments were recorded and processed as described for titration

experiments. The intensity ratio (I_{para}/I_{dia}) was determined for all observed amide proton resonances in the spectra of CcP with MTS-Cc (diamagnetic) or MTSL-Cc (paramagnetic) samples (Fig. S1). The $R_{2,para}$ was calculated as described previously [5,36]. For amides that gave an I_{para}/I_{dia} but for which the line width of the diamagnetic peak could be not obtained, the average value of all the calculated $R_{2,dia}$ values was used with a large error margin. For the amide peaks that disappear in the paramagnetic spectrum, an upper limit for I_{para} was set to two standard deviations of the noise level of the spectrum.

The calculated $R_{2,para}$ values were then converted into distances using (Eq. (1)):

$$r = \sqrt[6]{\frac{f_{bound}}{R_{2,para}} \frac{\gamma_H^2 g_e^2 \beta^2 \mu_0^2 (S+1)S}{240\pi^2} \left(4\tau_c + \frac{3\tau_c}{1+\omega_H^2\tau_c^2}\right)} \quad (1)$$

where r is the distance between the unpaired electron of the MTSL and a given amide proton of CcP, f_{bound} is the fraction of CcP bound to Cc (30% for 120 μM Cc; 73% for 290 μM), γ_H is the proton gyromagnetic ratio, g_e is the electronic g-factor, β is the Bohr magneton, μ_0 is the vacuum permeability, S is the spin quantum number for free electrons (1/2), τ_c is the rotational correlation time (estimated to be 16 ns [15]) and ω_H is the proton Larmor frequency. The calculated distances were divided into three classes: strongly affected residues for which the peaks had been completely broadened out in the paramagnetic spectrum and only an upper limit could be calculated, affected residues for which the peaks were visible in the paramagnetic spectrum (error margins were set to at least ±3 Å to account for experimental error) and residues that were too far away from the spin label to experience significant PRE, so only a lower limit could be calculated. These distances were then compared to back-calculated distances for a stereospecific, encounter or 30% encounter/70% stereospecific complex [5]. See Supplementary Methods for details.

3. Results and discussion

Previous paramagnetic NMR studies on the CcP–Cc complex were done by placing the probe on the surface of CcP and observing the paramagnetic effects in the spectra of Cc [5,15,23]. In order to observe the complex from the other side, the backbone assignment of CcP was obtained resulting in 240 assignments, 86% of assignable residues (Fig. S2). During this work, an independent assignment of CcP was published [37] with 197 assignments, a few of which were used to complement our data set. The 40 unassigned residues were either buried in the protein, probably experiencing incomplete back-exchange of the deuterons [38], or were within 5 Å of haem iron atom. Nonetheless, a sufficient coverage of the CcP surface was achieved to allow for mapping of interactions with spin-labelled Cc.

V28C was selected for spin labelling because it is located close to the binding interface between the two proteins and MTSL could be modelled into the crystal structure without resulting in steric clashes. To ensure that attachment of the tag in this location did not significantly disrupt complex formation, both WT and V28C-MTS Cc were titrated into ^{15}N, ^{2}H labelled CcP and CSP were monitored. Numerous resonances shifted in the spectrum, indicating a fast-exchange binding process. The K_B values were determined for the WT or MTS-V28C complex by fitting the CSP curves to a 1:1 binding model (Fig. 1). The K_B determined for the complex with WT Cc is $K_B = 2 \pm 1 \times 10^5\ M^{-1}$, which is the same within error as previously reported [39,40]. The binding constant for the complex with MTS-V28C was found to be the same within error, $K_B = 3 \pm 1 \times 10^5\ M^{-1}$. These values were then used to extrapolate average amide shifts, $\Delta\delta_{avg}$, for 100% bound CcP (Fig. S3). For the WT complex, the overall CSP pattern was similar to that described previously [41]. The CSPs for WT and MTS-V28C in this study were also identical within the error margins (±0.011 ppm) except for 20 peaks showing slightly larger differences (Table S2). The $\Delta\delta_{avg}$ values were used to create a CSP map (Fig. 2). For both WT and MTS-V28C Cc, the CSP effects on CcP were localized around the binding interface where Cc is expected to be in the stereospecific complex. The few peaks with significant differences in $\Delta\delta_{avg}$ for MTS-V28C (Table S2) are in the centre of the binding interface (square box in Fig. 2). However, overall the differences between the two CSP maps are small and the K_B values (Fig. 1) are the same within error, indicating that the effects of the tag on complex formation are minimal.

While CSP analysis can be used to determine how complexes interact and even provide restraints for modelling, PRE effects are much more sensitive to weak, transient interactions and lowly populated states due to their strong distance dependence (r^{-6}). This makes them much more suitable for studying encounter complexes. A PRE map was generated on the surface of CcP of PRE caused by MTSL-V28C Cc (Fig. 3). The strongest PRE effects were localized to the stereospecific binding interface, which is consistent with the CSP map (Fig. 2) but now the strongest effects (shown in red in both figures) are localized slightly differently. In the CSP map, the strongest interactions occur in a large patch in the bottom half of the binding interface, while this is shifted to a smaller patch at the top corner of the binding interface in the PRE map, near V28C. This difference is due to the different types of effects being

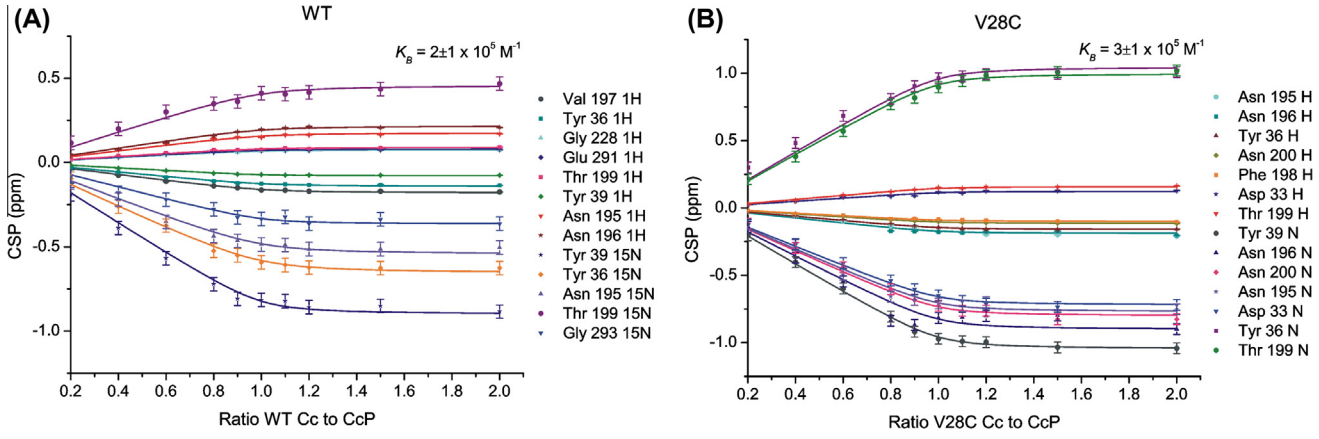

Fig. 1. Chemical shift perturbations for selected CcP residues in the ^{1}H or ^{15}N dimension during titration with WT Cc (A) or MTS-V28C Cc (B). The curves were fitted globally to a 1:1 binding model (described in Section 2) and the solid lines show the best fit when using a shared K_B value. These experiments were done in 20 mM NaPi, 100 mM NaCl (pH 6.0) at 293 K.

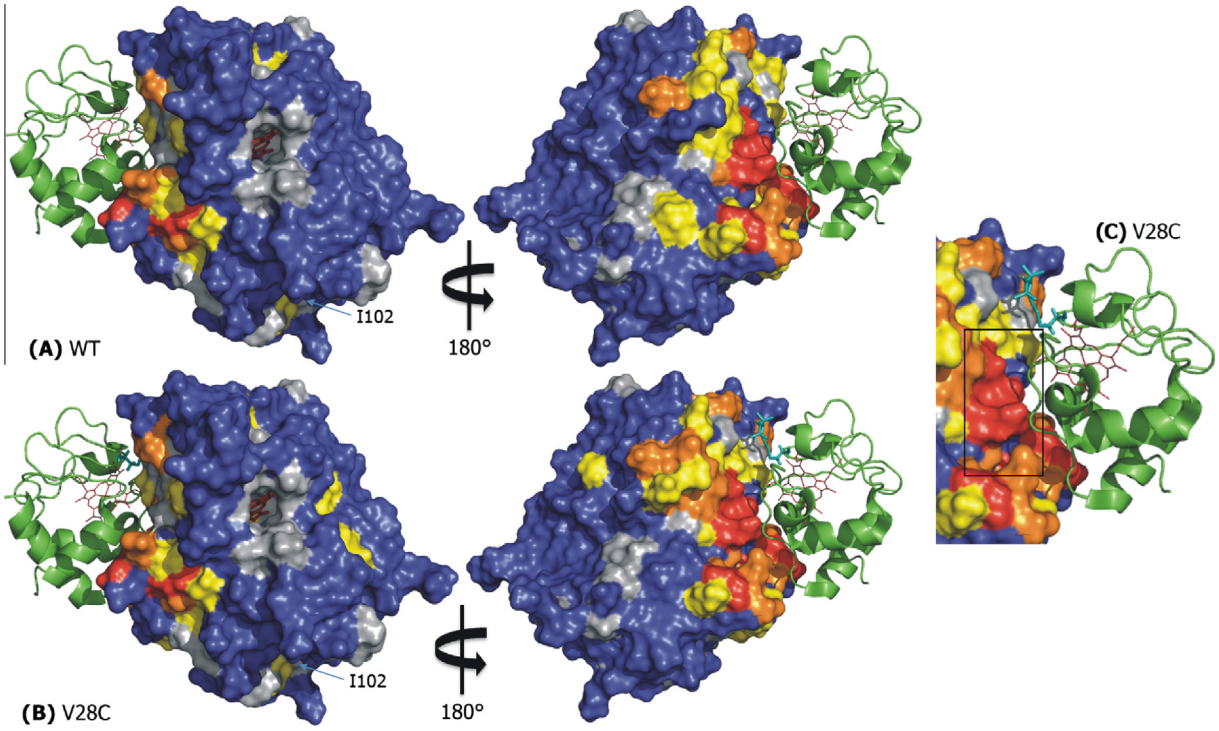

Fig. 2. Chemical shift perturbation map for ^{15}N, ^{2}H CcP C128A bound to WT (A) or MTS-V28C Cc (B and C), colour coded on a surface model of CcP (haem group in red sticks) in the stereospecific complex (PDB-entry 2GB8) [15]. Cc is shown in green ribbons with the haem group in red lines and MTSL-V28 is shown in teal sticks. CSP were extrapolated to 100% bound CcP. Residues with $\Delta\delta_{avg} \geqslant 0.06$ ppm are red, 0.04–0.06 ppm are orange, 0.02–0.04 ppm are yellow, 0–0.02 ppm are blue and with no data are grey. Residues with a large increase in $\Delta\delta_{avg}$ for MTS-V28C compared to WT are located in the black box.

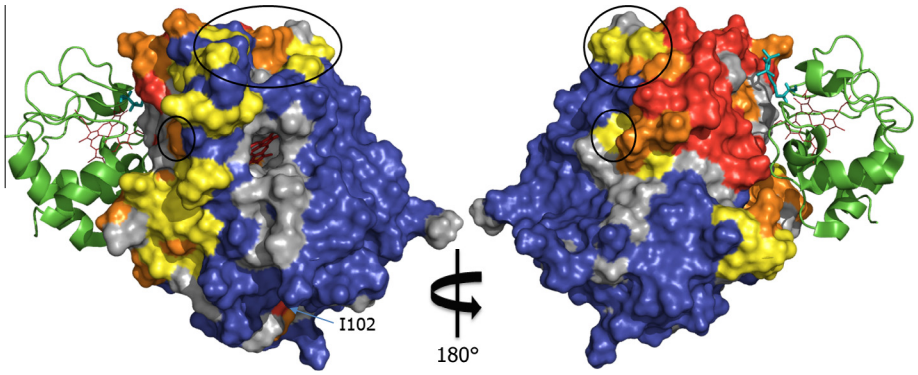

Fig. 3. PRE map for ^{15}N, ^{2}H CcP C128A in the presence of MTSL-V28C Cc, colour-coded on a surface model of CcP (haem group in red sticks) in the complex (PDB-entry 2GB8) [15]. Cc is shown in green ribbons with the haem group in red lines and MTSL-V28 is shown in teal sticks. The experimental PREs were measured in a sample in which 73% of CcP was bound to Cc. The PREs were then extrapolated to 100% bound CcP for this map. Residues with $\Gamma'_{2,para} \geqslant 100\ s^{-1}$ are red, $20\ s^{-1} < \Gamma'_{2,para} < 100\ s^{-1}$ are orange, $5\ s^{-1} < \Gamma'_{2,para} < 20\ s^{-1}$ are yellow, $\Gamma'_{2,para} \leqslant 5\ s^{-1}$ are blue and with no data are grey. Residue I102 is indicated with an arrow and residues 167, 188, 213, 230–243, 245, 247, 265 and 269 are located in the black circles.

observed; the CSP map shows the strongest interactions where the amide groups feel the strongest perturbation in their chemical environment while the strongest PRE effects occur close to V28C. Despite this slight difference in how the effects were focused, the majority of both types of effects were localized in the same area around the binding interface. The PRE effects however formed a much larger circumference around the interface of the stereospecific complex. This demonstrates clearly how much more sensitive PREs are for weak interactions and how they complement CSP data.

The PRE effects were converted to distances between affected residues and the paramagnetic centre. Previously, paramagnetic NMR studies on the CcP–Cc complex demonstrated that 30% of the complex population was in the encounter state [5,15], so the experimental data were expected to best match the predicted data for such a complex. For the PRE calculations, an estimate of 16 ns was used for the effective τ_c, the correlation time for the spin label-to-nucleus vector, which incorporates contributions from at least three types of mobility. First, there is the rotational diffusion of the entire CcP–Cc complex. Second, Cc rotates within the complex relative to CcP. The τ_c for Cc movement within the encounter complex has never been determined, so it is unknown how much it contributes to the overall τ_c. Third, the rotation of the spin label may contribute to the correlation time. This contribution is dependent on the distance between spin label and nucleus. The further the nucleus, the smaller the rotation angle of the spin label appears to be. Sixteen ns was used because it has been demonstrated before that this value gave a good fit to the experimental, PRE derived distances, suggesting that the overall rotation of the complex dominates τ_c [15].

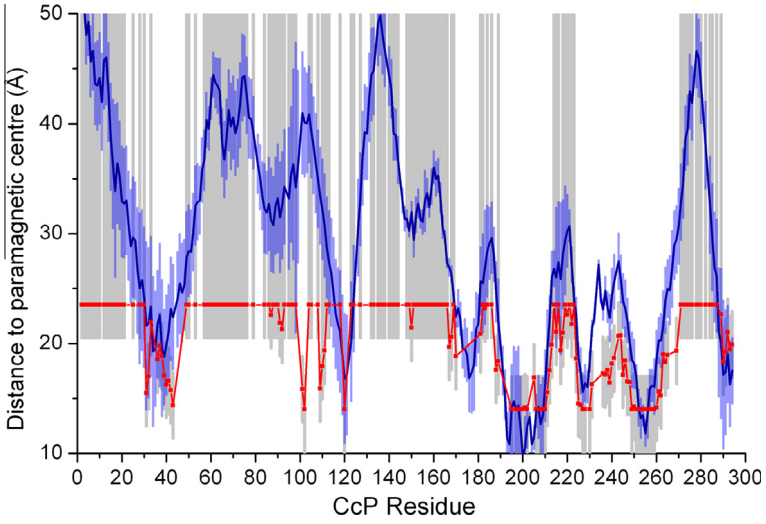

Fig. 4. Experimental and back-calculated averaged distances between CcP C128A amide protons and the paramagnetic centre in MTSL-V28C Cc plotted against the CcP residue number. The red squares represent the experimental distances with errors in grey bars. The average of back-calculated distances for a 30% encounter complexes for spin label rotamers A–C is shown as a blue line with a spread of two standard deviations shown in light blue bars (see Supplementary Methods for details on back-calculations). The experimental data were obtained with 73% CcP bound and extrapolated to 100%.

Because the orientation of the spin label in the complex is unknown and may vary, three widely spaced rotamers were used (Fig. S4) to back-calculate distances for six 30% encounter/70% stereospecific data sets, the average of which (± two standard deviations) was compared to the experimental data (Fig. 4) (see Supplementary Methods for calculation details). The PREs could be determined accurately between 14 and 23.5 Å (± ⩾3 Å), and in this range there was a good global agreement between the experimental and predicted distances for the 30% encounter complex. However, despite the large margins for error, there were significant differences for several residues: 43, 101, 102, 109, 167, 188, 205, 230–243, 245, 247, 265 and 269.

As mentioned above, to account for the flexibility of the spin label in the distance calculations, three very different rotamers were used to ensure sufficient margins of error were generated. The actual spin label orientations in the complex are unknown, so it cannot be excluded that distances for residues that are just outside the error margins are attributed to other spin label orientations. Residues 43 and 205 are directly in the binding interface of the stereospecific complex, and therefore sensitive to the spin label orientation.

The remaining residues that were more affected than predicted are in regions that border the binding interface (black circles in Fig. 3) or slightly towards the back of CcP (blue arrow in Fig. 3). Some of these also showed weak effects in the CSP map for WT (residues 101, 102, 109, 188, 230, 231, 236, 237) or MTS-V28C Cc (residues 101, 102, 109, 167, 188, 230, 235, 236) (Fig. 2) and similar effects were observed in the PRE data for 30% bound CcP (Fig. S5). The predicted data are based on a theoretical encounter complex simulation that was generated using an electrostatics-based Monte Carlo method [5]. Although it is a good representation, this model does not perfectly describe the encounter complex ensemble [6]. The observed discrepancies are relatively minor but significant, indicating that a larger data set will allow for better refinement of the model.

Interestingly, these effects were not observed by Bashir et al. in 2010 when they placed MTSL spin labels at ten locations on the surface of CcP and observed the PREs on Cc. In particular, MTSL was attached to L213C and S263C, which are located on either side of the region bordering the binding interface where we observe effects, but few effects were observed and none stronger than $I_{para}/I_{dia} = 0.8$. In that study MTSL was also attached to three residues close to I102 (V10, K97C and T137). MTSL at C137 showed weak effects ($I_{para}/I_{dia} = 0.8–1.0$) for most Cc residues. MTSL at C10 caused weak PRE around Cc residue 20, but MTSL at C97, which is located closest to I102, did not cause any significant effects on Cc [5]. It could be that the presence of MTSL at these locations interfered with encounter complex interactions at that site, resulting in weak/no observed PREs. It should be noted that the same holds true for this work; even though the CSP map and the affinity are hardly affected by the MTSL at V28C, it cannot be excluded that the spin label subtly influences the distribution of the Cc in the encounter complex.

This work highlights the importance of obtaining a comprehensive data set, by using paramagnetic tags located as several sites on both sides of the complex, in order to achieve a full understanding of how the proteins interact. Another consideration is the flexibility of MTSL. Although MTSL tags are great tools for mapping surface interactions, their inherent flexibility limits the precision of the data, so other, more rigid tags may be more useful for refinement of the encounter complex. Expanding these studies to including data form both sides of the complex and with different types of paramagnetic tags will thus allow for a more complete characterization of the CcP–Cc complex, including refining the encounter ensemble and possibly validating the proposed low-affinity binding site [42].

Acknowledgments

This work was supported by The Netherlands Organisation for Scientific Research (NWO), Grant 700.58.441. Measurement time was supported by the project Bio-NMR funded by the European Union, project number 261863.

Appendix A. Supplementary data

Supplementary data associated with this article can be found, in the online version, at http://dx.doi.org/10.1016/j.febslet.2014.03.055.

References

[1] Schilder, J. and Ubbink, M. (2013) Formation of transient protein complexes. Curr. Opin. Struct. Biol. 23, 911–918.

[2] Clore, G.M. (2011) Exploring sparsely populated states of macromolecules by diamagnetic and paramagnetic NMR relaxation. Protein Sci. 20, 229–246.
[3] Gardner, R.J., Longinetti, M. and Sgheri, L. (2005) Reconstruction of orientations of a moving protein domain from paramagnetic data. Inverse Probl. 21, 879–898.
[4] Longinetti, M., Luchinat, C., Parigi, G. and Sgheri, L. (2006) Efficient determination of the most favoured orientations of protein domains from paramagnetic NMR data. Inverse Probl. 22, 1485–1502.
[5] Bashir, Q., Volkov, A.N., Ullmann, G.M. and Ubbink, M. (2010) Visualization of the encounter ensemble of the transient electron transfer complex of cytochrome *c* and cytochrome *c* peroxidase. J. Am. Chem. Soc. 132, 241–247.
[6] Volkov, A.N., Ubbink, M. and van Nuland, N.A. (2010) Mapping the encounter state of a transient protein complex by PRE NMR spectroscopy. J. Biomol. NMR 48, 225–236.
[7] Fawzi, N.L., Doucleff, M., Suh, J.Y. and Clore, G.M. (2010) Mechanistic details of a protein–protein association pathway revealed by paramagnetic relaxation enhancement titration measurements. Proc. Natl. Acad. Sci. U.S.A. 107, 1379–1384.
[8] Hulsker, R., Baranova, M.V., Bullerjahn, G.S. and Ubbink, M. (2008) Dynamics in the transient complex of plastocyanin–cytochrome *f* from *Prochlorothrix hollandica*. J. Am. Chem. Soc. 130, 1985–1991.
[9] Xu, X., Reinle, W., Hannemann, F., Konarev, P.V., Svergun, D.I., Bernhardt, R. and Ubbink, M. (2008) Dynamics in a pure encounter complex of two proteins studied by solution scattering and paramagnetic NMR spectroscopy. J. Am. Chem. Soc. 130, 6395–6403.
[10] Xiong, P., Nocek, J.M., Griffin, A.K., Wang, J. and Hoffman, B.M. (2009) Electrostatic redesign of the [myoglobin, cytochrome b_5] interface to create a well-defined docked complex with rapid interprotein electron transfer. J. Am. Chem. Soc. 131, 6938–6939.
[11] Nocek, J.M., Knutson, A.K., Xiong, P., Co, N.P. and Hoffman, B.M. (2010) Photoinitiated singlet and triplet electron transfer across a redesigned [myoglobin, cytochrome b_5] interface. J. Am. Chem. Soc. 132, 6165–6175.
[12] Miyashita, O., Onuchic, J.N. and Okamura, M.Y. (2004) Transition state and encounter complex for fast association of cytochrome c_2 with bacterial reaction center. Proc. Natl. Acad. Sci. U.S.A. 101, 16174–16179.
[13] Harel, M., Cohen, M. and Schreiber, G. (2007) On the dynamic nature of the transition state for protein–protein association as determined by double-mutant cycle analysis and simulation. J. Mol. Biol. 371, 180–196.
[14] Kim, Y.C., Tang, C., Clore, G.M. and Hummer, G. (2008) Replica exchange simulations of transient encounter complexes in protein–protein association. Proc. Natl. Acad. Sci. U.S.A. 105, 12855–12860.
[15] Volkov, A.N., Worrall, J.A., Holtzmann, E. and Ubbink, M. (2006) Solution structure and dynamics of the complex between cytochrome *c* and cytochrome *c* peroxidase determined by paramagnetic NMR. Proc. Natl. Acad. Sci. U.S.A. 103, 18945–18950.
[16] Tang, C., Iwahara, J. and Clore, G.M. (2006) Visualization of transient encounter complexes in protein–protein association. Nature 444, 383–386.
[17] Bertini, I., Luchinat, C., Nagulapalli, M., Parigi, G. and Ravera, E. (2012) Paramagnetic relaxation enhancement for the characterization of the conformational heterogeneity in two-domain proteins. Phys. Chem. Chem. Phys. 14, 9149–9156.
[18] Luchinat, C., Nagulapalli, M., Parigi, G. and Sgheri, L. (2012) Maximum occurrence analysis of protein conformations for different distributions of paramagnetic metal ions within flexible two-domain proteins. J. Magn. Reson. 215, 85–93.
[19] Dasgupta, S. et al. (2011) Narrowing the conformational space sampled by two-domain proteins with paramagnetic probes in both domains. J. Biomol. NMR 51, 253–263.
[20] Bertini, I., Giachetti, A., Luchinat, C., Parigi, G., Petoukhov, M.V., Pierattelli, R., Ravera, E. and Svergun, D.I. (2010) Conformational space of flexible biological macromolecules from average data. J. Am. Chem. Soc. 132, 13553–13558.
[21] Bertini, I., Gupta, Y.K., Luchinat, C., Parigi, G., Peana, M., Sgheri, L. and Yuan, J. (2007) Paramagnetism-based NMR restraints provide maximum allowed probabilities for the different conformations of partially independent protein domains. J. Am. Chem. Soc. 129, 12786–12794.
[22] Bashir, Q., Scanu, S. and Ubbink, M. (2011) Dynamics in electron transfer protein complexes. FEBS J. 278, 1391–1400.
[23] Volkov, A.N., Bashir, Q., Worrall, J.A., Ullmann, G.M. and Ubbink, M. (2010) Shifting the equilibrium between the encounter state and the specific form of a protein complex by interfacial point mutations. J. Am. Chem. Soc. 132, 11487–11495.
[24] Pelletier, H. and Kraut, J. (1992) Crystal-structure of a complex between electron-transfer partners, cytochrome-*c* peroxidase and cytochrome-*c*. Science 258, 1748–1755.
[25] Northrup, S.H., Boles, J.O. and Reynolds, J.C. (1988) Brownian dynamics of cytochrome *c* and cytochrome *c* peroxidase association. Science 241, 67–70.
[26] Gabdoulline, R.R. and Wade, R.C. (2001) Protein–protein association: investigation of factors influencing association rates by brownian dynamics simulations. J. Mol. Biol. 306, 1139–1155.
[27] Teske, J.G., Savenkova, M.I., Mauro, J.M., Erman, J.E. and Satterlee, J.D. (2000) Yeast cytochrome *c* peroxidase expression in *Escherichia coli* and rapid isolation of various highly pure holoenzymes. Protein Expr. Purif. 19, 139–147.
[28] Goodin, D.B., Davidson, M.G., Roe, J.A., Mauk, A.G. and Smith, M. (1991) Amino-acid substitutions at tryptophan-51 of cytochrome-*c* peroxidase – effects on coordination, species preference for cytochrome-*c*, and electron-transfer. Biochemistry 30, 4953–4962.
[29] Vitello, L.B., Huang, M. and Erman, J.E. (1990) PH-dependent spectral and kinetic properties of cytochrome *c* peroxidase: comparison of freshly isolated and stored enzyme. Biochemistry 29, 4283–4288.
[30] Pollock, W.B., Rosell, F.I., Twitchett, M.B., Dumont, M.E. and Mauk, A.G. (1998) Bacterial expression of a mitochondrial cytochrome *c*. Trimethylation of lys72 in yeast iso-1-cytochrome *c* and the alkaline conformational transition. Biochemistry 37, 6124–6131.
[31] Morar, A.S., Kakouras, D., Young, G.B., Boyd, J. and Pielak, G.J. (1999) Expression of ^{15}N-labeled eukaryotic cytochrome *c* in *Escherichia coli*. J. Biol. Inorg. Chem. 4, 220–222.
[32] Vranken, W.F. et al. (2005) The CCPN data model for NMR spectroscopy: development of a software pipeline. Proteins 59, 687–696.
[33] Lescop, E., Schanda, P. and Brutscher, B. (2007) A set of BEST triple-resonance experiments for time-optimized protein resonance assignment. J. Magn. Reson. 187, 163–169.
[34] Grzesiek, S. et al. (1996) The solution structure of HIV-1 Nef reveals an unexpected fold and permits delineation of the binding surface for the SH3 domain of Hck tyrosine protein kinase. Nat. Struct. Biol. 3, 340–345.
[35] Kannt, A., Young, S. and Bendall, D.S. (1996) The role of acidic residues of plastocyanin in its interaction with cytochrome *f*. Biochim. Biophys. Acta Bioenerg. 1277, 115–126.
[36] Battiste, J.L. and Wagner, G. (2000) Utilization of site-directed spin labeling and high-resolution heteronuclear nuclear magnetic resonance for global fold determination of large proteins with limited nuclear overhauser effect data. Biochemistry 39, 5355–5365.
[37] Vanwetswinkel, S., van Nuland, N.A.J. and Volkov, A.N. (2013) Paramagnetic properties of the low- and high-spin states of yeast cytochrome *c* peroxidase. J. Biomol. NMR 57, 21–26.
[38] Volkov, A.N., Wohlkonig, A., Soror, S.H. and van Nuland, N.A.J. (2013) Expression, purification, characterization, and solution nuclear magnetic resonance study of highly deuterated yeast cytochrome *c* peroxidase with enhanced solubility. Biochemistry 52, 2165–2175.
[39] Volkov, A.N., Bashir, O., Worrall, J.A.R. and Ubbink, M. (2009) Binding hot spot in the weak protein complex of physiological redox partners yeast cytochrome *c* and cytochrome *c* peroxidase. J. Mol. Biol. 385, 1003–1013.
[40] Worrall, J.A., Kolczak, U., Canters, G.W. and Ubbink, M. (2001) Interaction of yeast iso-1-cytochrome *c* with cytochrome *c* peroxidase investigated by [^{15}N, ^{1}H] heteronuclear NMR spectroscopy. Biochemistry 40, 7069–7076.
[41] Volkov, A.N. and van Nuland, N.A. (2008) Solution NMR study of the yeast cytochrome *c* peroxidase: cytochrome *c* interaction. J. Biomol. NMR 56, 255–263.
[42] Volkov, A.N., Nicholls, P. and Worrall, J.A.R. (2011) The complex of cytochrome *c* and cytochrome *c* peroxidase: The end of the road? Biochim. Biophys. Acta Bioenerg. 1807, 1482–1503.